

Theory of dichroic X-ray tomography and laminography

Authors

Matthew A. Marcus^{a*}

^aAdvanced Light Source, Lawrence Berkeley Laboratory, 1 Cyclotron Road, Berkeley, CA, 94720, United States

Correspondence email: mamarcus@lbl.gov

Funding information Office of Basic Energy Sciences, US Department of Energy (contract No. DE-AC02-05CH11231).

Synopsis The theory of the generalization of tomography and laminography to materials with linear or circular dichroism is discussed using a formalism derived from the filtered back-projection method of reconstruction. For linearly-dichroic samples, three polarizations or three tilt angles are required in order to have enough information for reconstruction, while circularly-dichroic samples require two tilts.

Abstract Dichroic tomography is a 3D imaging technique in which the polarization of the incident beam is used to induce contrast due to the magnetization or orientation of a sample. The aim is to reconstruct not only the optical density but the dichroism of the sample. The theory of dichroic tomographic and laminographic imaging in the parallel-beam case is discussed as well as the problem of reconstruction of the sample's optical properties. The set of projections resulting from a tomographic/laminographic measurement is not sufficient to reconstruct the magnetic moment for magnetic circular dichroism unless additional constraints are applied or data are taken at two or more tilt angles. For linear dichroism, three polarizations or three tilt angles are required to provide enough information to reconstruct without constraints. Possible means of applying constraints are discussed. Furthermore, it is shown that for linear dichroism, the basic assumption that the absorption through a ray path is the integral of the absorption coefficient, defined on the volume of the sample, along the ray path, is not correct when dichroism or birefringence is strong. This assumption is fundamental to tomographic methods..

Keywords: tomography;laminography;x-ray linear dichroism;x-ray circular dichroism.

1. Introduction

Throughout the history of their use, X-rays have been used to make two-dimensional, and later, three-dimensional images encoding the distribution of elements or chemical species, which are expressed as scalar quantities. However, in many cases, one is interested either in magnetic moments (vector) or crystal orientation (tensor). The imaging of magnetic structures has been of major importance in the study of spintronic and other magnetic materials, and many methods have been developed for imaging magnetization in two dimensions. One important class of such methods makes use of the phenomenon of magnetic circular dichroism (MCD), in which the X-ray absorbance of a material differs between left- and right-circular polarization by an amount depending on the local magnetization (Fischer, 2014, Stöhr & Siegmann, 2006). This effect is readily used to create two-dimensional images in various sorts of X-ray microscopes such as ptychographs (Yu *et al.*, 2018) or photoelectron emission microscopes (Rana *et al.*, 2020). Note that these two papers are only examples; many more exist in the literature. However, only recently has there been work in which the magnetic order, as a three-dimensional vector, been imaged in three dimensions (Donnelly *et al.*, 2017).

Another important class of materials is crystals, in which the orientation is an important part of the microstructure and plays an important role in understanding the properties and functions of crystalline materials. For instance, teeth are made of apatite, which is not a particularly strong or durable material, but the nanostructure of enamel makes them wear-resistant enough to last a lifetime (Stifler *et al.*, 2021). While diffractive methods such as electron backscatter diffraction and X-ray diffraction tomography can provide very useful information in two and three dimensions, they have limitations in sample thickness (electron diffraction) or resolution on the nanoscale or fail if the material is not perfectly crystalline, as is often the case for biominerals. What is wanted is a method which can image the orientation of a crystalline material, over cubic microns of volume, with sub-micron or nanoscale resolution. Although methods such as PEEM-PIC mapping (DeVol *et al.*, 2014) and dichroic ptychography (Chang *et al.*, 2020, Lo *et al.*, 2021, Gao *et al.*, 2020) provide the requisite resolution and sampling area in two dimensions, it can be very difficult to image orientations in three dimensions.

Dichroic tomography is an extension of the well-known technique of X-ray computed tomography, in which a sample is rotated in an X-ray beam and, at each of a set of rotation angles, a projection image (radiograph) is captured. This set of images is processed to produce a 3D reconstruction of the absorption density of the sample. In dichroic tomography, the incident beam is polarized, and so additional contrast is provided due to the crystal orientation (linear dichroism) or magnetization (circular).

The purpose of this paper is to discuss the theory of how the properties of the sample map onto the projected images, and how one might reconstruct not only an overall absorption at each voxel, but the anisotropy. This leads to considerations such as:

1. What assumptions must we make and under what conditions are they valid?
2. How many polarizations need we use? Can we get the whole set of parameters (three components of magnetization, or full orientation and magnitude of linear dichroism)?
3. What is the difference between computed tomography geometry (CT, rotation axis perpendicular to beam) and computed laminography (CL, rotation axis at an angle to the beam other than 90°)?

The next section goes over a number of definitions and discuss the framework and formalism used for the math. Then I'll specify some assumptions being made and what they imply, including a review of filtered back-projection, after which comes the actual derivations.

This paper was originally written in the context of soft X-ray scanning transmission X-ray microscopy (STXM), but the results should apply to hard X-rays and to full-field imaging methods.

2. Preliminaries

This section is where definitions and formalism are laid out.

2.1. Assumptions

First, some assumptions:

A1: The absorption through the material, from source to detector, may be described by Beer's law applied to each voxel along the line of sight. Thus, there is such a thing as a volume absorbance, which has an angular and polarization dependence for a dichroic material.

The result of a normal tomographic reconstruction is the volume absorbance of the set of voxels defined by positions in the sample, $\mu(x, y, z)$. Thus, the beam intensity after passing through a small thickness dl of material at this position is attenuated by a factor of $1 - \mu(x, y, z)dl$. For an isotropic material, this quantity is independent of beam direction or polarization, an assumption implicit in all standard tomographic reconstruction algorithms. This assumption is fundamental to most, if not all tomographic reconstruction algorithms.

An important way in which this assumption is violated is if the polarization of the beam changes as the beam propagates through the material. As an extreme example, shown in Figure 1, consider a material which is so strongly dichroic that a small thickness of it acts like a polarizer. If the incident polarization is vertical but a grain has a vertical absorbing axis so it acts like a horizontal polarizer, the transmitted intensity is low. If, however, a grain oriented at 45° is placed before the

original grain, the interposed grain turns the polarization, and now up to 1/4 of the incident beam goes through. If the order of the grains is switched, the transmission drops again. This shows that a simple line-integral treatment of absorption does not work in strong dichroism conditions. The transmission is not a scalar, but a tensor described not by a line integral but by a product of non-commuting matrices. This problem does not occur in the MCD case because the polarization remains left or right circular as the beam passes through the sample (Zhao *et al.*, 1998). The propagation of X-rays through a linearly-dichroic material is described in a number of places including (Chang *et al.*, 2020).

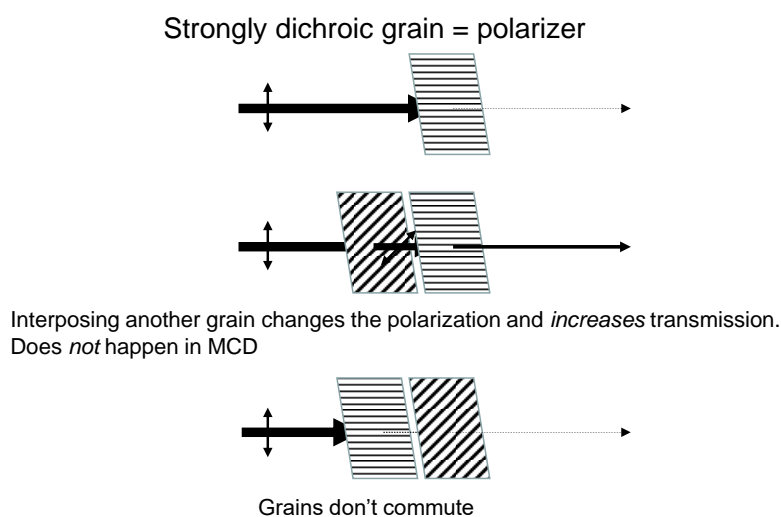


Figure 1 A case in which Beer's law applied to a line integral of absorption doesn't work. The hatching direction shows the direction of the E-field passed by a grain, acting as a polarizer.

What can be done to make A1 true or nearly true? One way is to operate in a regime of weak dichroism and birefringence. This of course can cause trouble with noise and artefacts, but at least guarantees that the polarization remains nearly unchanged through the sample. Note that operating at an energy below or near the dichroic peak, even if the dichroism of absorption is small, may not be appropriate because the sample may still be birefringent enough to act like a stack of waveplates and scramble the polarization. In analysis, it may be possible to adopt some kind of tensor formalism, especially if real and imaginary parts of the transmission are known as would be the case if the projections are derived from ptychography. It may also be possible to come up with an algorithm incorporating a multislice model as the forward model in an iterative loop.

The next assumption refers to the use of ptychography:

A2: Ptychography is just a high-resolution form of STXM. The result of ptychographic reconstruction at a given beam direction and polarization is an image which reduces to an optical density at each pixel which is given by a line integral of the volume absorbance along the beam direction. The volume absorbance at a voxel is that of a bulk piece of material of the same composition and orientation as that of the material of the voxel.

In the presence of linear dichroism, this assumption should be applied carefully. The reconstruction of the transmitted field in principle needs to take into account the tensor nature of the index of refraction (Chang *et al.*, 2020). However, once the reconstruction is done, the squared magnitude of the transmitted field plays the role that transmission does in STXM.

Now comes an assumption which may not be necessary but makes the math simpler:

A3. No missing angles. It is assumed possible to rotate the sample through a full 360° over as many angles as necessary for reconstruction.

The next assumption involves terms which will be defined below, so readers who don't know what back-projection is should read to that section and come back. This assumption is:

A4. The back-projection derived from all the projections uniquely maps onto the projections and therefore contains all the information in the projections, which is all the information there is.

This is actually a theorem, rather than just an assumption. The proof is as follows: The contribution to the back-projection from a single pixel of any of the projections is a line in real space, extending along the beam direction corresponding to that projection. Thus, its Fourier transform is a sheet in Fourier space, oriented perpendicular to the beam direction and passing through the origin. Now consider the Fourier transform of a single back-projection, which is the contribution to the back-projection from a single rotation. Since the lines from all points on the detector are parallel, they contribute to the same sheet in Fourier space, which now contains the Fourier transform of the projection. Since all the sheets are unique, it follows that the Fourier transform of the back-projection can be unfolded to give the Fourier transforms of each projection, which can be inverted to yield the set of projections. For a finite number of rotations, the sheets intersect each other at a set of measure zero compared with any one sheet, so a point on a sheet corresponds uniquely to a point on a projection's Fourier transform.

Finally, an assumption which provides an important simplification for dichroic CT/CL:

A5: The incident beam is collimated, so its direction, and hence the polarization vector is the same for all points in the sample.

Thus, we do not consider cone-beam imaging or imaging with a focused probe for which the thickness of the sample is significant compared with the depth of focus.

2.2. Definitions

Next, a number of definitions:

The method consists of rotating the sample in the beam while taking radiographs. Each radiograph is processed assuming Beer's Law to produce the projected absorption along the beam path. These are called *projections*, and are parameterized by the rotation angle γ and any other variables such as polarization.

If the rotation axis is perpendicular to the beam, then we have *computed tomography (CT)* geometry and each projection may be regarded as a stack of projections of 2D slices. Otherwise, we have *computed laminography (CL)* geometry and no such slicing is possible – the whole volume must be reconstructed at once. While CL is more complex than CT, and as we shall see, has an intrinsic limitation due to missing information, it is often the only way to work with samples that are sheet-like in geometry, as CT will result in projections in which the sample is probed on-edge. This case results in ranges of rotation angles in which the data are useless because the sample is effectively too thick to see through. Also, for circular dichroism, CL offers the potential of detecting all three components of magnetization, while CT misses the component along the rotation axis.

Two coordinate systems will be used. One is the *lab coordinate system* (or reference frame), in which the beam comes from a fixed direction, the detector is in a fixed position, and the sample rotates. The other is the *sample coordinate system* (or reference frame) in which the sample is fixed and the source and detector pirouette around it. This is the coordinate system in which we want the eventual reconstructions to be defined.

It is assumed that the absorption through the sample (a projection) is described for each angle and voxel by a local *effective absorption coefficient*

$$r(\vec{X}; \gamma, \chi) = \ln(I_0 / I) = \int dl \mu(\vec{x}(l); \gamma, \chi) \quad (1)$$

where l is the length along a path extending to a given point on the detector, $\vec{x}(l)$ is the position in the sample (in its own coordinate system) corresponding to l and the position on the detector \vec{X} , γ is the rotation angle and χ is the polarization, specified either as an angle with respect to the horizontal (in the lab coordinate system) or a handedness of circular polarization. The phenomena we're probing are *MCD* (magnetic circular dichroism) or *XLD* (X-ray linear dichroism). XLD may come from crystalline anisotropy, in which case the objective is to solve for the crystal orientation at each voxel, or the second-order linear dichroism of an antiferromagnet, in which case the goal is to solve for the order parameter.

The method of reconstruction we will consider involves the creation of back-projections, made by adding up single back-projections for each rotation angle. A *single back-projection*, parameterized by the rotation angle is made by projecting a projection back through the sample to create a 3D density:

$$p(\vec{x}; \gamma, \chi) = \int r(\vec{X} - l\hat{n}; \gamma, \chi) dl \quad (2)$$

where \vec{x} is a position in the sample volume, r is the projection at a given rotation angle, \hat{n} is the beam direction in the sample reference frame, and l is the length along the beam from the sample voxel \vec{x} to the plane of the detector.

The *back-projection* is the sum of the set of single back-projections, and looks like the object with a blurry halo around it. This halo, at least in the isotropic case, can be removed by a Fourier filtering procedure, resulting in a *filtered back-projection* as an approximation of the original sample.

To get from a set of projections or a back-projection to the unknown parameters of the sample, we must use some sort of mathematical method, which essentially does a large linear-algebra problem. Reconstruction by filtered back-projection (FBP) is the core of one family of methods used for isotropic samples. The other major family of methods considers the set of local absorptions per pixel as a large vector of unknowns, which is related by a linear matrix operation to the set of projections, considered as a larger vector of observations. This is essentially a linear least-squares problem, but the response matrix is huge. The vector of unknowns has as many elements as there are voxels and the vector of observations has a length equal to the product of the number of angles and the number of pixels on the detector. Thus, for a small case of a 200x200x200-voxel sample volume, 360 rotations and a 200x200 pixel detector, we have 8×10^6 unknowns and 1.44×10^7 observations, so the matrix would have 1.16×10^{14} elements. Even on a supercomputer cluster, it would be impractical to store and invert such a matrix, even though it is sparse. Instead, *iterative least-squares methods* such as SIRT (Simultaneous Iterative Reconstruction Technique (van der Sluis & van der Vorst, 1987)) are used. Although these methods are better in some senses than FBP methods and have largely taken over the field, the argument above shows that back-projections contain all the information there is, so FBP methods can be used to investigate the conditions under which there is enough information to reconstruct anisotropic samples.

We will see that the local absorption coefficient varies with rotation angle according to a trigonometric series including sines and cosines of the rotation angle and twice the rotation angle. If one wants the coefficients in such an expansion, one way to do it is to average the function with a weight of $\sin \gamma$, $\cos \gamma$, $\sin 2\gamma$, or $\cos 2\gamma$. Similarly, the projections $p(\vec{x}, \gamma)$ will include trig-function variation, so one can get all the available information by taking averages over γ such as $\langle p(\vec{x}, \gamma) \cos \gamma \rangle$ with the angle brackets denoting an angular average over rotation angle γ . These shall be denoted as *weighted back-projections*, and the trig-function coefficients of $\mu(\vec{x}, \gamma)$ as *moments*. For some of the analysis, it will be more convenient to expand in terms of $\exp(im\gamma)$, with m ranging from -1 to 1 (MCD) and -2 to 2 (XLD). This is, of course, equivalent to an expansion in sines and cosines.

Much of the mathematical work was done using Mathematica (Wolfram Research, 2021). In particular, the `MatrixRank[]` and `Eigenvalues[]` functions were used in order to evaluate the number of independent equations represented in some linear systems.

3. Dichroism framework

At this point, we can start to create the framework in which we work. First, I will define some geometry. This is where assumption A5 (beam direction is everywhere the same) comes in. Figure 2 shows the assumed geometry, which shows the general CL case and the notation for the relevant angles. This geometry was originally considered for a tomographic electron-microscope sample holder, but is general enough to be applied to other mechanical arrangements.

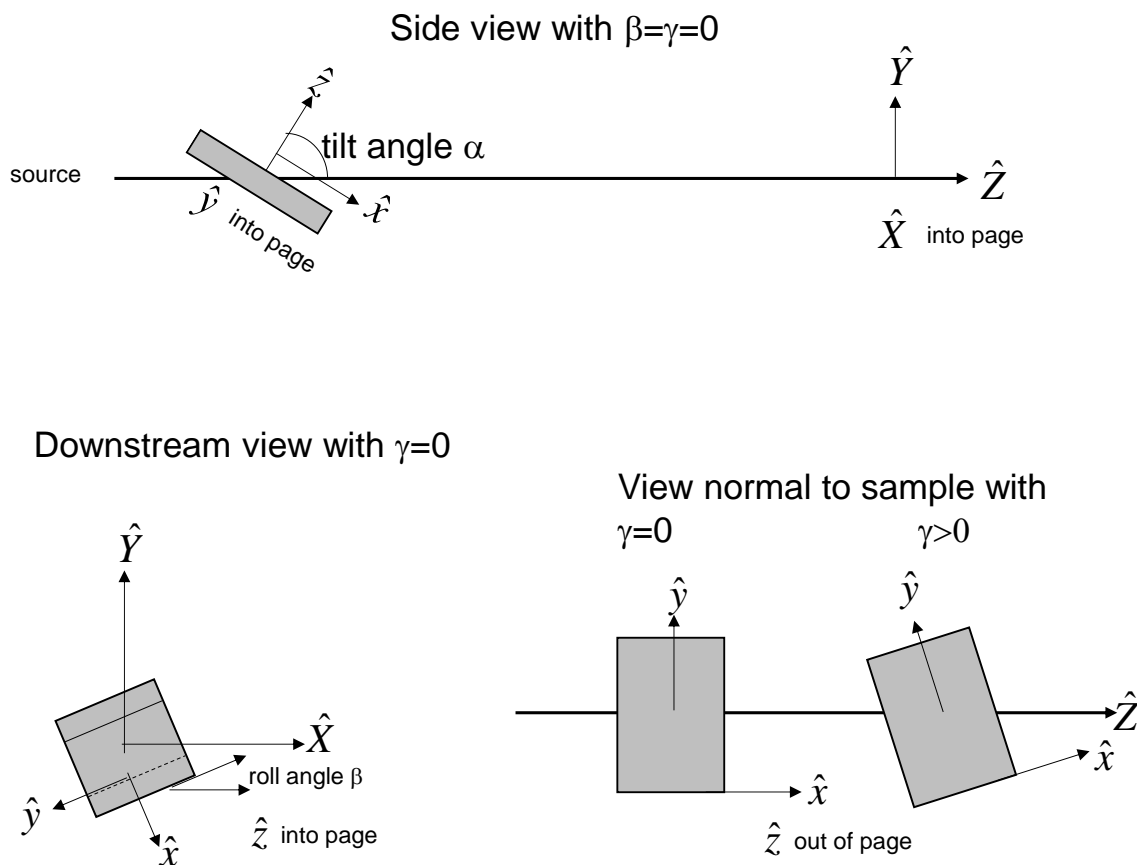


Figure 2 Geometry of the measurement. The unit vectors \hat{x} , \hat{y} , \hat{z} define the sample coordinate system with \hat{z} the rotation axis. Lab coordinate axes are \hat{X} , \hat{Y} , \hat{Z} with \hat{Z} being the beam direction. The three angles provided by the mechanics are α , the angle between the rotation axis and the beam, so $\alpha = 90^\circ$ is CT mode., β , a roll angle about the beam axis, and γ the rotation angle, which is the only angle that varies between projections. Further, the polarization in XLD measurements is defined in terms of χ , the angle between the polarization vector and the horizontal (\hat{X}). The entire sample holder rotates about the X axis (α), the plate holding the grid wags up and down by angle β , and the sample, idealized as a thin object such as a TEM grid, rotates in its own plane by angle γ . The rotation specified by β is equivalent to rolling the sample about the beam axis. This action can be mimicked by rolling the polarization and detector about the beam axis, so β has no non-trivial effect. Thus, we will take it to be 0 in the following. Now we can start to assemble the $(\hat{x}\hat{y}\hat{z})$ orthonormal

triad in lab coordinates. Start with $\alpha = 90^\circ$; $\beta = \gamma = 0$. Inspection of Figure 2 shows that the $(\hat{x}\hat{y}\hat{z})$ triad in lab coordinates is:

$$\begin{pmatrix} \hat{x} \\ \hat{y} \\ \hat{z} \end{pmatrix} \Big|_{90^\circ, 0, 0} = \begin{pmatrix} 0 & 0 & 1 \\ 1 & 0 & 0 \\ 0 & 1 & 0 \end{pmatrix}. \quad (3)$$

The determinant of this matrix is 1, showing that the parity of the sample coordinate system as illustrated in Figure 2 is the same as that of the lab system. The first rotation to apply is α , which differs from the other two in that it is done in the lab system, since the whole holder moves. This is a rotation about X , which mixes \hat{Y} and \hat{Z} , so we have

$$\begin{pmatrix} \hat{x} \\ \hat{y} \\ \hat{z} \end{pmatrix} \Big|_{\alpha, 0, 0} = \begin{pmatrix} 0 & 0 & 1 \\ 1 & 0 & 0 \\ 0 & 1 & 0 \end{pmatrix} \begin{pmatrix} 1 & 0 & 0 \\ 0 & \sin \alpha & \cos \alpha \\ 0 & -\cos \alpha & \sin \alpha \end{pmatrix} = \begin{pmatrix} 0 & -\cos \alpha & \sin \alpha \\ 1 & 0 & 0 \\ 0 & \sin \alpha & \cos \alpha \end{pmatrix}. \quad (4)$$

Note that since we started with $\alpha = 90^\circ$, we have to adjust the right-hand rotation matrix to refer to a rotation of $90^\circ - \alpha$. Figure 2 shows the geometry with α between 0 and 90° and we see that (4) gets the sign right.

The next step is to apply the in-plane γ rotation which mixes \hat{x} and \hat{y} :

$$\begin{pmatrix} \hat{x} \\ \hat{y} \\ \hat{z} \end{pmatrix} \Big|_{\alpha, 0, \gamma} = \begin{pmatrix} \cos \gamma & \sin \gamma & 0 \\ -\sin \gamma & \cos \gamma & 0 \\ 0 & 0 & 1 \end{pmatrix} \begin{pmatrix} \hat{x} \\ \hat{y} \\ \hat{z} \end{pmatrix} \Big|_{90^\circ, 0, 0}, \quad (5)$$

Using Mathematica to do the algebra results in the final matrix:

$$R_{\alpha 0 \gamma} = \begin{pmatrix} \hat{x} \\ \hat{y} \\ \hat{z} \end{pmatrix} \Big|_{\alpha, 0, \gamma} = \begin{pmatrix} \sin \gamma & -\cos \alpha \cos \gamma & \sin \alpha \cos \gamma \\ \cos \gamma & \cos \alpha \sin \gamma & -\sin \alpha \sin \gamma \\ 0 & \sin \alpha & \cos \alpha \end{pmatrix}. \quad (6)$$

This is the matrix which, when multiplying a vector in lab coordinates, yields its equivalent in sample coordinates. Even if the assumptions about the order of rotations is wrong, the use of this rotation matrix should still let us determine whether a given set of measurements is enough to perform reconstructions. The inverse of this matrix is:

$$R_{\alpha 0 \gamma}^{-1} = \begin{pmatrix} \sin \gamma & \cos \gamma & 0 \\ -\cos \alpha \cos \gamma & \sin \alpha \sin \gamma & \sin \alpha \\ \cos \gamma \sin \alpha & -\sin \alpha \sin \gamma & \cos \alpha \end{pmatrix} = R_{\alpha 0 \gamma}^T. \quad (7)$$

Next, we will need the polarization and the beam direction, expressed in the sample frame of reference, in which $\hat{x}, \hat{y}, \hat{z}$ are the basis vectors. The beam direction, which I have been denoting by \hat{n} , is given by the third column of the rotation matrix:

$$\hat{n} \cdot \begin{pmatrix} \hat{x} \\ \hat{y} \\ \hat{z} \end{pmatrix} = \begin{pmatrix} \sin \alpha \cos \gamma \\ -\sin \alpha \sin \gamma \\ \cos \alpha \end{pmatrix} \quad (8)$$

and the polarization vector, again in sample coordinates, is

$$\hat{e} = R_{\alpha\gamma} \hat{E}_\chi = \begin{pmatrix} \sin \gamma \cos \chi - \cos \gamma \cos \alpha \sin \chi \\ \cos \gamma \cos \chi + \sin \gamma \cos \alpha \sin \chi \\ \sin \alpha \sin \chi \end{pmatrix}. \quad (9)$$

With the geometry in place, we can put in the physics of dichroism. What follows is a long string of formulas set out here for later use. For MCD, the effective absorption coefficient is linearly-related to the dot product of the beam direction and the magnetization, so can be expressed as (Fischer, 2014):

$$\mu(\vec{x}, \gamma, s) = \mu_{nd}(\vec{x}) + s \vec{m}(\vec{x}) \cdot \hat{e}(\gamma) \quad (10)$$

where $s = \pm 1$ depending on the handedness of the polarization, \vec{m} is the product of the magnetization and a dichroism proportionality constant and μ_{nd} is a background, non-dichroic absorption. Just from imaging, it's impossible to separate the magnitude of the magnetization from the amount of dichroism a given magnetization produces. However, it's likely in many systems that this response coefficient is proportional to μ_{nd} . In particular, if $\mu_{nd} = 0$ for a voxel, that voxel is empty so \vec{m} must also vanish. If we represent \vec{m} in polar coordinates, $\vec{m} = m(\sin \theta \cos \phi, \sin \theta \sin \phi, \cos \theta)$, we have

$$\mu = \mu_0 + sm(\sin \alpha \sin \theta \cos(\gamma + \phi) + \cos \alpha \cos \theta). \quad (11)$$

Note that if we subtract the projections done at one polarization from corresponding projections done at the other, we remove μ_{nd} , leaving the dichroic contribution. Decomposing this into single trig functions, we have

$$\begin{aligned} \mu &= C_0 + C_1 \cos \gamma + S_1 \sin \gamma \\ C_0 &= \mu_{nd} + sm_z \cos \alpha \\ C_1 &= sm_x \sin \alpha \\ S_1 &= -sm_y \sin \alpha \end{aligned} \quad (12)$$

or, equivalently,

$$\begin{aligned} \mu &= \mu_{-1} e^{-i\gamma} + \mu_0 + \mu_1 e^{i\gamma} \\ \mu_{-1} &= s \sin \alpha (m_x + im_y) / 2 \\ \mu_0 &= \mu_{nd} + sm_z \cos \alpha \\ \mu_1 &= s \sin \alpha (m_x - im_y) / 2 \end{aligned} \quad (13)$$

Here, $m_{x,y,z}$ are the components of \vec{m} in sample coordinates. We see that in CT mode ($\alpha = 90^\circ$), we lose information about one of the components of the magnetization, m_z . This is because in CT mode, the sample z axis is always perpendicular to the beam, so there is no dichroism due to magnetization in that direction. In CL mode, if we can get the three moments we can get the scaled magnetization \vec{m} .

For linear dichroism, the formalism is more complex. Many materials of interest are optically uniaxial due to their crystallinity (calcite, for instance) or nearly so (aragonite and vaterite). If we assume uniaxiality with an orientation unit vector \hat{p} , then the absorption may be described according to Malus' law as

$$\mu = \mu_{nd} + \mu_d (\hat{p} \cdot \hat{e})^2 \quad (14)$$

where μ_d measures the strength of the dichroism. Expressing the orientation in polar coordinates as

$$\hat{p} = \hat{x} \sin \theta \cos \phi + \hat{y} \sin \theta \sin \phi + \hat{z} \cos \theta \quad (15)$$

we have,

$$\mu = \mu_{nd} + \mu_d (\sin \chi \cos \theta + \cos \chi \sin \theta \sin(\gamma + \phi))^2, \quad (16)$$

which looks similar to the equation we had for MCD, (11), except that the angle-dependent term is squared. The math simplifies a bit if we assume that μ_d has the same sign everywhere and re-express the dichroism as

$$\vec{p}' = \sqrt{|\mu_d|} \hat{p} \quad (17)$$

which makes the basic equation read

$$\mu = \mu_{nd} \pm (\vec{p}' \cdot \hat{e})^2 \quad (18)$$

where the \pm sign is there to deal with the cases of positive or negative dichroism. In that case, we have

$$\begin{aligned} \mu &= C_0 + C_1 \cos \gamma + C_2 \cos 2\gamma + S_1 \sin \gamma + S_2 \sin 2\gamma \\ C_0 &= \mu_{nd} \pm (3(p_x'^2 + p_y'^2) + 2p_z'^2 + (p_x'^2 + p_y'^2 - 2p_z'^2)(\cos 2\alpha + \sin^2 \alpha \cos 2\chi)) / 8 \\ C_1 &= \pm 2p_z' \sin \alpha \sin \chi (p_y' \cos \chi - p_x' \sin \chi \cos \alpha) \\ S_1 &= \pm 2p_z' \sin \alpha \sin \chi (p_x' \cos \chi + p_y' \sin \chi \cos \alpha) \\ C_2 &= \pm \frac{1}{8} (p_y'^2 - p_x'^2) ((3 + \cos 2\alpha) \cos 2\chi + 2 \sin^2 \alpha) \mp p_x' p_y' \cos \alpha \sin 2\chi \\ S_2 &= \pm \left(\frac{1}{2} (p_y'^2 - p_x'^2) \cos \alpha \sin 2\chi + \frac{p_x' p_y'}{4} ((3 + \cos 2\alpha) \cos 2\chi + 2 \sin^2 \alpha) \right) \end{aligned} \quad (19)$$

or in exponential notation,

$$\begin{aligned}
\mu &= \mu_{-2}e^{-2i\gamma} + \mu_{-1}e^{-i\gamma} + \mu_0 + \mu_1e^{i\gamma} + \mu_2e^{2i\gamma} \\
\mu_{-2} &= \mp \frac{p'_x - ip'_y}{4} (\cos \chi + i \cos \alpha \sin \chi)^2 \\
\mu_{-1} &= \mp (p'_x - ip'_y) p'_z \sin \alpha \sin \chi (\cos \alpha \sin \chi - i \cos \chi) \\
\mu_0 &= \mu_{nd} \pm (3(p_x'^2 + p_y'^2) + 2p_z'^2 + (p_x'^2 + p_y'^2 - 2p_z'^2)(\cos 2\alpha + \sin^2 \alpha \cos 2\chi)) / 8 \\
\mu_1 &= \mp (p'_x + ip'_y) p'_z \sin \alpha \sin \chi (\cos \alpha \sin \chi + i \cos \chi) \\
\mu_2 &= \mp \frac{p'_x + ip'_y}{4} (\cos \chi - i \cos \alpha \sin \chi)^2
\end{aligned} \tag{20}$$

Note that with Mathematica, the easiest way to extract these coefficients is to evaluate weighted integrals such as $\mu_2 = (1/2\pi) \int_0^{2\pi} \mu(\gamma) \exp(-2i\gamma) d\gamma$.

From the above, we see that from the ratio of, for instance, μ_2 to μ_1 we could extract p'_z , and from $\mu_{\pm 1}$, $p'_{x,y}$ and then from μ_0 , the non-dichroic background μ_{nd} . This only works in the case of laminography ($\alpha \neq 90^\circ$) and an oblique polarization. Thus, if we can somehow reconstruct the moments, we can get the information we want, in most cases without needing to switch polarizations (XLD) or tilt angles (MCD). We will see later on, however, that we can't actually get all the moments without adding extra information.

There is another way to describe XLD which is mathematically more elegant than the above, but does not easily enforce the assumption of uniaxiality. The absorption is described by a symmetric tensor, which is proportional to the imaginary part of the dielectric tensor:

$$\mu = \hat{e}^T \cdot \mathbf{Q} \cdot \hat{e} = \hat{e}^T \cdot \begin{pmatrix} Q_1 & Q_4 & Q_5 \\ Q_4 & Q_2 & Q_6 \\ Q_5 & Q_6 & Q_3 \end{pmatrix} \cdot \hat{e} \tag{21}$$

so the unknowns form a 6-component vector $(Q_1, Q_2, Q_3, Q_4, Q_5, Q_6)$. This one-index notation is what's used in other fields such as solid mechanics (strain, stress). The advantage of this representation is that, unlike the uniaxial vector representation, the equations are linear in the unknowns so matrix algebra can be used, just as in the MCD case. Also, there's no \pm to keep track of. The moments are thus,

$$\begin{pmatrix} \mu_{-2} \\ \mu_{-1} \\ \mu_0 \\ \mu_1 \\ \mu_2 \end{pmatrix} = S(\chi) \begin{pmatrix} Q_1 \\ Q_2 \\ Q_3 \\ Q_4 \\ Q_5 \\ Q_6 \end{pmatrix}$$

$$S(\chi) = \begin{pmatrix} \frac{-(c_\chi + is_\chi c_\alpha)^2}{4} & \frac{(c_\chi + is_\chi c_\alpha)^2}{4} & 0 & \frac{i(c_\chi + is_\chi c_\alpha)^2}{2} & 0 & 0 \\ 0 & 0 & 0 & 0 & s_\alpha s_\chi (c_\chi + ic_\alpha s_\chi) & is_\alpha s_\chi (c_\chi + ic_\alpha s_\chi) \\ \frac{c_\chi^2 + c_\alpha^2 s_\chi^2}{2} & \frac{c_\chi^2 + c_\alpha^2 s_\chi^2}{2} & s_\alpha^2 s_\chi^2 & 0 & 0 & 0 \\ 0 & 0 & 0 & 0 & s_\alpha s_\chi (c_\chi - ic_\alpha s_\chi) & -is_\alpha s_\chi (c_\chi - ic_\alpha s_\chi) \\ \frac{-(c_\chi - is_\chi c_\alpha)^2}{4} & \frac{(c_\chi - is_\chi c_\alpha)^2}{4} & 0 & \frac{-i(c_\chi - is_\chi c_\alpha)^2}{2} & 0 & 0 \end{pmatrix} \quad (22)$$

where $c_\chi = \cos \chi$; $s_\chi = \sin \chi$; $c_\alpha = \cos \alpha$; $s_\alpha = \sin \alpha$. Similarly, in MCD, we have

$$\begin{pmatrix} \Delta\mu_{-1} \\ \Delta\mu_0 \\ \Delta\mu_1 \end{pmatrix} = S_{MCD} \begin{pmatrix} m_x \\ m_y \\ m_z \end{pmatrix} = (1/2) \begin{pmatrix} \sin \alpha & -i \sin \alpha & 0 \\ 0 & 0 & 2 \cos \alpha \\ \sin \alpha & i \sin \alpha & 0 \end{pmatrix} \begin{pmatrix} m_x \\ m_y \\ m_z \end{pmatrix} \quad (23)$$

where $\Delta\mu_m = \mu_m|_{s=+1} - \mu_m|_{s=-1}$ is the dichroic contrast. We will use these matrices later. To get more of a feel for the relation between polarization and available information content, we can evaluate the S -matrix for XLD at a couple of specific polarization angles. For horizontal polarization ($\chi = 0$), vertical polarization ($\chi = 90^\circ$) and $\chi = 45^\circ$, we have

$$\begin{aligned}
S_{XLD}(\chi = 0) &= \begin{pmatrix} -1/4 & 1/4 & 0 & i/2 & 0 & 0 \\ 0 & 0 & 0 & 0 & 0 & 0 \\ 1/2 & 1/2 & 0 & 0 & 0 & 0 \\ 0 & 0 & 0 & 0 & 0 & 0 \\ -1/4 & 1/4 & 0 & -i/2 & 0 & 0 \end{pmatrix} \\
S_{XLD}(\chi = 90^\circ) &= \begin{pmatrix} c_\alpha^2/4 & -c_\alpha^2/4 & 0 & -ic_\alpha^2/4 & 0 & 0 \\ 0 & 0 & 0 & 0 & ic_\alpha s_\alpha & -c_\alpha s_\alpha \\ c_\alpha^2/2 & c_\alpha^2/2 & s_\alpha^2 & 0 & 0 & 0 \\ 0 & 0 & 0 & 0 & -ic_\alpha s_\alpha & -c_\alpha s_\alpha \\ c_\alpha^2/4 & -c_\alpha^2/4 & 0 & -ic_\alpha^2/4 & 0 & 0 \end{pmatrix} \\
S_{XLD}(\chi = 45^\circ) &= \begin{pmatrix} \frac{(c_\alpha - i)^2}{8} & \frac{-(c_\alpha - i)^2}{8} & 0 & \frac{-i(c_\alpha - i)^2}{4} & 0 & 0 \\ 0 & 0 & 0 & 0 & \frac{s_\alpha(1 + ic_\alpha)}{2} & \frac{s_\alpha(i - c_\alpha)}{2} \\ \frac{3 + \cos(2\alpha)}{8} & \frac{3 + \cos(2\alpha)}{8} & \frac{\sin^2 \alpha}{2} & 0 & 0 & 0 \\ 0 & 0 & 0 & 0 & \frac{s_\alpha(1 - ic_\alpha)}{2} & \frac{s_\alpha(-i - c_\alpha)}{2} \\ \frac{(c_\alpha + i)^2}{8} & \frac{-(c_\alpha + i)^2}{8} & 0 & \frac{i(c_\alpha + i)^2}{4} & 0 & 0 \end{pmatrix} \quad (24)
\end{aligned}$$

We see that for $\chi = 0$, there is no information available for Q_3, Q_5 and Q_6 , which are the three tensor components of Q which involve the sample rotation axis. This is because, as seen from the sample's point of view, the polarization vector has no component in that direction for any γ .

For the MCD case, if we can measure all three moments, we can get all the information we want. However, for XLD without some additional assumption or information such as perhaps another polarization, we can't because there are 6 unknowns and only 5 observables. One possibility is to constrain to uniaxiality. Unfortunately, this constraint is a non-linear condition, mainly that two of the eigenvalues of Q are equal. Such a condition can't be implemented simply by, for instance, adding another row to S . Another possibility is to take another scan at an energy at which there is no dichroism, then assume based on the composition of the sample a scaling relation between the observed absorption coefficient at that energy and the isotropic part at the energy at which the dichroic CT/CL is performed. That effectively gives the trace of Q , adding a sixth component to the moments vector and a sixth row to S . We can test this by adding another row to S consisting of (1,1,1,0,0,0) and asking Mathematica for the rank of the now 6x6 matrix. The result is 6, showing that adding the constraint on the trace of Q fixes the under-determination problem, given knowledge of the moments. However, this only works if the sample is homogeneous and its optical properties are very well-known, perhaps from measurements on a polycrystal.

If we use another polarization, then we have 10 observables and 6 unknowns, so one might think that there are plenty of constraints. Actually, the problem is just determined. Proof: Set up the equations for two polarizations:

$$\begin{pmatrix} M(\chi_1) \\ M(\chi_2) \end{pmatrix} = \begin{pmatrix} S(\chi_1) \\ S(\chi_2) \end{pmatrix} \mathbf{Q} \quad (25)$$

where $M(\chi)$ is the column vector of moments for polarization χ and \mathbf{Q} is the column vector of absorption-tensor values. The matrix that multiplies \mathbf{Q} has 10 rows and 6 columns and can be assembled in Mathematica with the `Catenate[]` function. The `MatrixRank[]` function then reports that the rank is 6, just enough to solve for \mathbf{Q} .

At this point, it appears that we can find all three components of the scaled magnetization (CL mode only) or all six components of the absorption tensor for XLD using two polarization (LCP/RCP for MCD, two angles for XLD). However, this is contingent on being able to measure all three (MCD) or five (XLD) moments. We will see that this is actually not possible; the set of projections does not yield enough information. This deficit is over and above the missing cone in Fourier space that's inevitable in CL and which we will discuss later.

4. Back-projections and filtered back-projections

So far, it is now established that for MCD, reconstructing three moments of the absorption will provide all the information we need. For XLD, five moments would be sufficient if another constraint, such as uniaxiality, could be imposed. Now we need to figure out how to do this reconstruction, and whether and under what circumstances it's possible. We have already been using assumption A1 (ability to describe transmission in terms of a local absorption) and A5 (collimated beam). From here on, we will use A3 (no missing angles) and A4 (back-projections map into projections). However, before getting into the details of reconstruction, I will digress a bit to discuss the missing information in laminography, even for isotropic materials.

4.1. Missing information in laminography

One way to see that there must be missing information in laminography is to consider the method applied to a sample which is layered normal to the rotation axis but is uniform in-plane. For this case, rotation of the sample produces no variation of absorption; all projections are the same. Therefore, the layering is completely unresolved and all one gets is the total absorption through the sample.

The effect may be described by considering the back-projection in Fourier space. Recall that the back-projection is the sum of many single back-projections. Each of these has the form of a bundle of lines of density extended along the beam direction for the given projection. The Fourier transform of such a bundle is a sheet oriented perpendicular to the beam direction. When the sample is rotated, the sheet, in the sample's reference frame, rotates about the sample rotation axis, resulting in a double

cone within which there is no intensity. Thus, Fourier components within this cone are not sampled and no information is available about them. The mathematics of this phenomenon are shown explicitly by (Myagotin *et al.*, 2013) and by (Matsuo *et al.*, 1993). Examples of the reconstruction artefacts produced by this missing cone are shown by (Fisher *et al.*, 2019) in their demonstration of cone-beam laminography on a laboratory apparatus. Note that although the missing cone was demonstrated mathematically in the context of filtered back-projection reconstruction, the effect is independent of reconstruction method because it's a real gap in the available information. Theorem A4 shows that no reconstruction algorithm will dig up information that filtered back-projection can't. As an example, the reconstructions shown by (Fisher *et al.*, 2019) were done using an iterative least-squares algorithm, not filtered back-projection.

4.2. Reconstruction of moments

We have seen that the unknown object may be described in terms of effective absorption coefficients which oscillate as a function of rotation angle γ . Suppose we want to derive a generalization of filtered back-projection which can reconstruct not just an angle-independent μ but all the moments $\{\mu_i\}$. The back-projection corresponding to a single point of isotropic absorption at position $\vec{x} = \vec{x}_0$ looks like a double cone of non-zero values with the vertex at position \vec{x}_0 , oriented along the rotation axis. The intensity is concentrated at this vertex because the lines from the different angles crowd together, thus producing a power-law singularity. This is why the unfiltered back-projection resembles the object but with a 'haze' around each point. Now consider the (unphysical) case in which only one of the non-zero moments appears, $\mu_i(\vec{x}) = \delta(\vec{x} - \vec{x}_0)\delta_{im}$. The back-projection produced by the "object" is still a double cone, but modulated with angle by a factor of $e^{im\gamma}$. Unlike the back-projection from an isotropic point absorber, the double cone with $m \neq 0$ does not have a concentration at the vertex. The appearance of the back-projections of point objects was verified by simulation using the ASTRA toolbox (Van Aarle *et al.*, 2016). If we perform the back-projection of an object having intensity in all the moments $\mu_m, m \in [-2, 2]$ (XLD) or $m \in [-1, 1]$ (MCD), we get a complex mixture of contributions from all the μ_i . The μ_0 component will still be concentrated at points where μ_0 is high, but simulations show that the other moments contribute significantly.

Now, if we perform the back-projection by first weighting each projection by $e^{-im\gamma}$, we change the μ_m moment into what looks like μ_0 , somewhat the way a lock-in amplifier converts an oscillating signal into a DC one by mixing it with a reference of the same frequency. Thus, we could imagine performing a series of filtered back-projections on weighted projections, then solving for the moments. This process is illustrated graphically in Figure 3. In this example, real-valued trig-function weightings are shown, rather than complex exponentials.

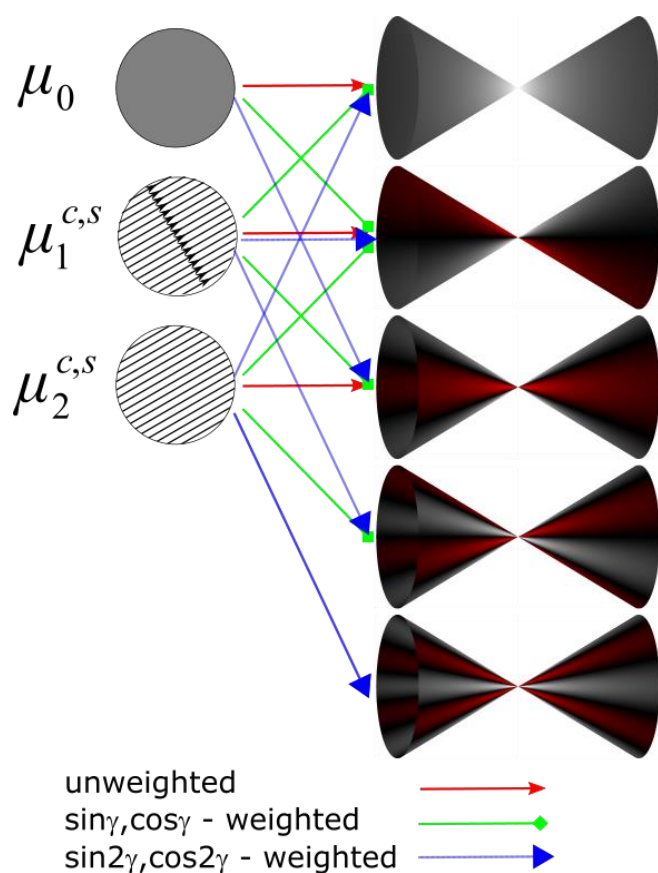


Figure 3 A graphical representation of the effect of performing $\sin, \cos(n\gamma)$ -weighting on the contributions to weighted back-projections from the components of the absorption density. The double cones represent weighted projections of a point object with positive values shown as grey (brighter = higher), negative values shown as red and 0 as black. Note that the resulting angular components in the projections go up to $n=4$. The weightings are shown as arrows connecting moments of the absorption (the circles on the left) with the resulting contributions to the back-projections.

Here, the uniformly-shaded disk represents isotropic absorption, the single-headed arrows represent moments of order 1 and the lines with no arrows represent moments of order 2. The double cones represent back-projections of point objects with varying angular dependence. We see that the contributions of moments of order up to ± 2 , when weighted, yield contributions to order ± 4 . Thus, in order to go from observables (the back-projections) to unknowns (the moments), we must perform what is effectively a matrix inversion.

4.2.1. Generalized filtered back-projection

In ordinary filtered back-projection, the filtering is done by computing the FT of the double-conical back-projection and using the inverse (where it's not 0) as a deconvolution filter. Here, we

generalize to a multicomponent problem. For this purpose, it is easier to work with complex components, as in Eq. (20), than sines and cosines as in Figure 3. The weighted projections from an isotropic point object at $\vec{x} = 0$ are given by:

$$P_n(\vec{x}) = \int_0^{2\pi} d\gamma \exp(in\gamma) \int \delta(\vec{x} - \hat{n}(\gamma)l) dl \quad (26)$$

where $\hat{n}(\gamma)$ is the direction along the ray when the projection angle is γ and l is a path length along the ray. The projections from an extended object are sums of convolutions of P_n with the angular components μ_m , $m = -2 \dots 2$:

$$\begin{aligned} p_n(x) &= \sum_{m=-2}^2 \int_0^{2\pi} d\gamma \exp(i(n+m)\gamma) \int dl \mu_m(\vec{x} + l\hat{n}(\gamma)) \\ &= \sum_{m=-2}^2 (\mu_m \otimes P_{n+m}) \end{aligned} \quad (27)$$

where P_n is given by

$$P_n(x) = \int_0^{2\pi} d\gamma e^{in\gamma} \int_{-\infty}^{\infty} dl \delta(\vec{x} - \hat{n}(\gamma)l) . \quad (28)$$

What we need is the FT of this, in order to do the deconvolution. The back-projection is a sum of lines all going through the origin. Therefore, the FT is a sum of sheets in k -space, produced by taking one sheet, tilted with its normal tilted at an angle α to the rotation (\hat{z}) axis, and weighted by the $e^{im\gamma}$ factor. Thus, we can write the FT of weighted back-projection P_m as

$$\begin{aligned} F_m &= \frac{1}{2\pi} \int_0^{2\pi} d\gamma e^{im\gamma} \delta(k_z \sin \alpha + \cos \alpha [k_x \cos \gamma + k_y \sin \gamma]) \\ &= \frac{1}{2\pi} \int_0^{2\pi} d\gamma e^{im\gamma} \delta(k_z \sin \alpha + \cos \alpha k_t \cos(\gamma - \psi)) \\ &= \frac{e^{im\psi}}{2\pi} \int_0^{2\pi} d\gamma e^{im\gamma} \delta(k_z \sin \alpha + \cos \alpha k_t \cos \gamma) \end{aligned} \quad (29)$$

with the substitution $k_t = \sqrt{k_x^2 + k_y^2}$ and ψ is the azimuthal angle of \vec{k} , thus

$k_x = k_t \cos \psi$; $k_y = k_t \sin \psi$. Next, we express the delta function as the well-known integral

$\delta(x) = (1/2\pi) \int_{-\infty}^{\infty} dw \exp(ixw)$ and reverse the order of integrations:

$$F_m = \frac{e^{im\psi}}{(2\pi)^2} \int_{-\infty}^{\infty} dw \exp(iwk_z \sin \alpha) \int_0^{2\pi} d\gamma \exp(i(m\gamma + wk_t \cos \alpha \cos \gamma)) . \quad (30)$$

The second integral is one of the many integral forms of the J Bessel function, so:

$$F_m = \frac{e^{im\psi}}{2\pi i^m} \int_{-\infty}^{\infty} dw \exp(iwk_z \sin \alpha) J_m(wk_t \cos \alpha) \quad (31)$$

Mathematica can evaluate this, with result:

$$F_m(\vec{k}) = \begin{cases} \frac{e^{im\gamma} T_m(z/t)}{\pi \sqrt{t^2 - z^2}} & t \geq |z| \\ 0 & t < |z| \end{cases} \quad (32)$$

where $z = k_z \sin \alpha$; $t = k_t \cos \alpha$, $T_m(x)$ is the Chebyshev polynomial of the first kind, and this form is true for negative m as well as positive. The missing cone falls naturally out of the math without needing to be put in by hand. The result for $m=0$ is the one well-known for filtered back-projection, derived for laminography by (Matsuo *et al.*, 1993).

We need to be careful in evaluating F for $k_z = 0$. At $k_t = k_z = 0$, the function is undefined because $\lim_{k_t \rightarrow 0} \lim_{k_z \rightarrow 0} F_m = 0$ but $\lim_{k_z \rightarrow 0} \lim_{k_t \rightarrow 0} F_m$ is infinite. It seems to be standard to take the value of the reciprocal transform (F_m^{-1} in our case) to be 0 at the origin of k -space. However, the limit for $k_z = 0, k_t \neq 0$ is a bit tricky. One could evaluate it by doing careful calculations using (32) but it's easier to go back to (29) which for $k_z = 0$ reads:

$$F_m(k_t, k_z = 0) = \frac{e^{im\gamma}}{2\pi} \int_0^{2\pi} d\gamma e^{im\gamma} \delta(k_t \cos \alpha \cos \gamma). \quad (33)$$

The argument of the delta function goes through 0 at $\gamma = \pi/2, 3\pi/2$ with slopes $-k_t \cos \alpha, k_t \cos \alpha$. Therefore, the integral is

$$F_m(k_t, k_z = 0) = \frac{e^{im\gamma}}{2\pi k_t \cos \alpha} (e^{3im\pi/2} + e^{im\pi/2}) \\ = \begin{cases} \frac{e^{im\gamma} (-1)^{m/2}}{\pi k_t \cos \alpha} & m \text{ even} \\ 0 & m \text{ odd} \end{cases} \quad (34)$$

Now that we have the FTs, we find that the FT of the weighted back-projections is:

$$\bar{p}_n(\vec{k}) = \sum_{m=-2}^2 F_{n+m}(\vec{k}) \bar{\mu}_m \quad (35)$$

where the over-bar represents Fourier transformation. This is a matrix equation in thin disguise, with the unknown vector being $\{\bar{\mu}_m\}$. Thus, the procedure would be to do 3D FFTs of the set of weighted back-projections, then, for all points in k -space not in the missing cone, multiply the vector of FFTs by the inverse matrix, leaving the missing-cone values set to 0, then inverting the FFT. The matrix algebra becomes easier if we re-express (35) in a form that separates out the phase factors:

$$\bar{p}_n(\vec{k}) = \sum_{m=-2}^2 e^{im\gamma} G_{n+m}(\vec{k}) e^{im\gamma} \bar{\mu}_m \quad (36)$$

where $G_n = e^{-im\gamma} F_n$; $G_{-n} = G_n$. Thus, if we multiply \bar{p}_n by $e^{-im\gamma}$ and $\bar{\mu}_n$ by $e^{im\gamma}$, we get a form with a real, symmetric matrix:

$$\begin{pmatrix} \tilde{p}_{-2} \\ \tilde{p}_{-1} \\ \tilde{p}_0 \\ \tilde{p}_1 \\ \tilde{p}_2 \end{pmatrix} = \begin{pmatrix} G_0 & G_1 & G_2 & G_3 & G_4 \\ G_1 & G_0 & G_1 & G_2 & G_3 \\ G_2 & G_1 & G_0 & G_1 & G_2 \\ G_3 & G_2 & G_1 & G_0 & G_1 \\ G_4 & G_3 & G_2 & G_1 & G_0 \end{pmatrix} \begin{pmatrix} \tilde{\mu}_{-2} \\ \tilde{\mu}_{-1} \\ \tilde{\mu}_0 \\ \tilde{\mu}_1 \\ \tilde{\mu}_2 \end{pmatrix} \quad (37)$$

where quantities with a tilde are the $e^{\pm im\gamma}$ -multiplied over-barred quantities.

There is a special case which needs to be considered, which is that of $\vec{k} = 0$, which will be one of the points sampled in the discrete FT. The value of the FFT at the 0 point is the sum over the imaged volume of the operand. Consider a ‘sample’ which is uniform within some volume outside which it’s empty, and has only an m ’th moment, which means that it has an unphysical $\mu = \exp(im\gamma)$. Then, for the LHS of (37) we have $\tilde{\mu}_n = \delta_{nm}$ and $\tilde{p}_n = C\delta_{nm}$ where C is a constant. To evaluate this constant, it’s probably easiest to simulate the back-projections through a uniformly-filled volume and sum up all voxels of the back-projection. Since the proportionality of $\tilde{\mu}_n$ and \tilde{p}_n holds for all values, it follows that the matrix in (37) must reduce to the identity matrix times C for the $\vec{k} = 0$ point.

All of the above is aimed at the problem of reconstructing the moments μ_m of the absorption coefficients. From that, we can go back to the formalism starting at (10) to get the material properties represented by \vec{m} or Q_i . For instance, the development leading to (20) relates the moments to a solution for uniaxial linear dichroism with a single oblique polarization in laminography, while that leading to (13) shows that the scaled magnetization can be solved for with two polarizations in CL mode.

Can we actually carry out this program?

4.2.2. Missing information

There is a major problem with the above approach if one tries to use it with a single polarization and tilt. It turns out that the G matrix in (37) is singular. That means that it’s possible to add to the $\tilde{\mu}_m$ coefficients an extra contribution $A(\vec{k})u_m(z, t)$ where $A_m(\vec{k})$ is any function in k -space and $u_m(z, t)$ is one of the eigenvectors corresponding to a 0 eigenvalue (there is one for the 3x3 MCD case and three for XLD) of the matrix to be inverted. Several speculative workarounds can be proposed. One possibility is to solve the equation in the singular-value decomposition (SVD) sense, which gives a solution, and one with the smallest norm, but probably not *the* solution. It seems from numerical experiments that ‘extra’ components yield ‘bleed’ outside the boundaries of the object. Such ‘bleed’ may be expected to increase the norm of the solution and so not appear in the SVD solution. Yes, this

is a weak argument. Another possible solution is to ask that outside of some support volume, all components of μ are zero. How would we get that support volume? Perhaps one could use a conventional method of reconstruction other than filtered back-projection, maybe at an energy at which dichroism is negligible. Some version of shrink-wrapping might also be possible. Thus, we can frame the problem as a minimization problem:

$$\sum_{\vec{k}} (P_k - FM_k)^2 + \lambda \sum_{\vec{x} \notin V} \left| \sum_{\vec{k}} e^{i\vec{k} \cdot \vec{x}} M_k \right|^2 = \min \quad (38)$$

where P_k and M_k are the vectors $\{\bar{P}_m(\vec{k})\}$ and $\{\bar{\mu}_m(\vec{k})\}$, F is the matrix of $F_n(\vec{k})$, V is the support volume and λ is a multiplier. I don't know if this support requirement is sufficient to define M_k uniquely. Differentiating (38) with respect to $M_{\vec{q}}$ yields

$$F_{\vec{q}} M_{\vec{q}} - P_{\vec{q}} + \lambda \sum_{\vec{x} \notin V} \sum_{\vec{k}} e^{i(\vec{q}-\vec{k}) \cdot \vec{x}} M_k^* = 0 \quad . \quad (39)$$

Note that we have M entering as M and its complex conjugate M^* , so the matrix in the linear solution of this problem is of size $5 \times N_k \times 2$ on a side where N_k is the number of points in k -space. If we zero-pad to twice the size in each direction to avoid convolution artefacts, then we have $N_k = 8N_v$, where N_v is the number of voxels. This is clearly too large to be handled by the usual methods, so, just as in the normal least-squares methods, it will have to be done by iteration. The obvious way to do that is to move the λ term to the RHS and consider the $M_{\vec{q}}$ as the next value in the iteration, but that doesn't solve the problem of $F_{\vec{q}}$ being singular. If we bring back to the LHS only the $\vec{k} = \vec{q}$ term in the inner summation, we get something that isn't singular:

$$(F_{\vec{q}} + \lambda N_{out}) M_{\vec{q}}^{next} = P_{\vec{q}} - \lambda \sum_{\vec{x} \notin V} \sum_{\vec{k} \neq \vec{q}} e^{i(\vec{q}-\vec{k}) \cdot \vec{x}} M_k^* = 0 \quad (40)$$

where $M_{\vec{q}}^{next}$ is the next estimate of $M_{\vec{q}}$, N_{out} is the number of voxels in the excluded volume, and the sum over wavevectors in the RHS excludes $\vec{k} = \vec{q}$. The value of λ may need to be adjusted so that $\lambda N_{out} \ll G_0(\vec{q})$, the diagonal element of the F -matrix. It is not known whether this will converge or for what values of λ . It's possible that this iterative method may help with the artefacts caused by the missing cone, which extend out from the actual body of the sample. Since we're back to iteration, it's not obvious why we would want to use the weighted-moments method at all. This consideration highlights the idea that the weighted-moments method is intended more as an exploratory tool for identifying what's possible, than the basis of a practical algorithm.

For XLD, one extra bit of information we have is that for many, if not most cases of interest, the optical properties are uniaxial, so we could write the absorption coefficient tensor as

$$Q(\vec{x}) = \hat{p}^T \hat{p} \mu_{\parallel}(\vec{x}) + (1 - \hat{p}^T \hat{p}) \mu_{\perp}(\vec{x}) \quad (41)$$

where \hat{p} is the orientation direction, μ_{\parallel} is the absorption coefficient parallel to that direction, and μ_{\perp} is that perpendicular. Counting up degrees of freedom yields four independent variables, i.e. two constraints. Since the matrix for XLD has three vanishing eigenvalues, it appears that uniaxiality does not provide enough constraint to remove the degeneracy. Also, the relationship between the weighted moments, in real space, is not simply linear, so linear methods don't work, as shown in (19).

Suppose we add polarizations to get more information in XLD. As we did previously in discussing the connection between material parameters and moments of μ , we can make a pile of the matrices connecting $\{\bar{p}_m\}$ and \mathbf{Q} and test for rank. The resulting equation, in block-matrix form, is

$$\begin{pmatrix} \bar{P}(\chi_1) \\ \dots \\ \bar{P}(\chi_{n_\chi}) \end{pmatrix} = \begin{pmatrix} GS(\chi_1) \\ \dots \\ GS(\chi_{n_\chi}) \end{pmatrix} (\bar{Q}) \quad (42)$$

where \bar{Q} is the set of 6 independent tensor components of the absorption in Fourier space, n_χ is the number of polarizations and $S(\chi)$ is the k -independent 5x6 matrix which relates the tensor components to the angular components. Does that solve the problem? Again, we can ask Mathematica for the rank of the piled matrix. We find that the rank is 2 with one polarization, 4 with two polarizations and 6 with three. This means that we can in principle do the reconstruction with three polarizations, but they have to be carefully chosen. Two obvious choices are $(0^\circ, 45^\circ, 90^\circ)$ and $(90^\circ, -30^\circ, 210^\circ)$, but both are rank-deficient. Adding 36° to all the angles fixes the problem and gets back to a rank of 6. There's nothing magic about this choice; it's just one that yields a rank-6 matrix.

It should be noted that since the matrix has more rows than columns, we're now in the domain of a least-squares solution, though one of manageable size for each k -point, rather than the global one with hundreds of trillions of elements.

For MCD, we do have a missing-information problem as was noted by (Donnelly *et al.*, 2018). While it's true that the rank of S_{MCD} is 3 for CL, the rank of the 3x3 matrix corresponding to the G -matrix in (37) is 2, so we can't solve for all components of \vec{m} . We can't add polarizations because in MCD we only have two, and we're using both to get rid of the non-dichroic term. This rank is preserved on multiplying on the right by S_{MCD} . Thus, we need a constraint. On certain length scales, many materials have magnetizations either only in the plane of a film or perpendicular to it. If the film plane is the rotation plane, then the perpendicular case corresponds to $\vec{m} = (0, 0, m_z)$. In this case, tomography as we have been discussing it fails to deliver 3D information. If a CT geometry is used, the magnetization is perpendicular to the beam direction, so no dichroic signal will be observed. If CL is used, the missing cone in Fourier space includes the direction normal to the

film, so no depth resolution will be obtained. However, this case is somewhat artificial; the domain walls or other boundaries between areas of differing m_z have local moments out of the normal direction, so the only information we can get comes from places where the constraint is violated. For the in-plane case, the nullspace of the GS matrix contains one vector, which has components along \hat{x} , \hat{z} directions. This implies that anything one might add to $\vec{m}(\vec{x})$ that still satisfies the linear equation of the reconstruction will inevitably have a component in the \hat{z} -direction, which we're not allowing. Unfortunately, many of the interesting structures we would want to look at such as skyrmions or hopfions obey no such constraints, as shown for instance in Figure 3 of (Donnelly *et al.*, 2018).

One way around the problem is to use multiple tilt angles, by analogy with the multiple polarizations used for XLD. The calculation must be done carefully because the matrix G depends on the tilt angle for a given point in Fourier space so each block in the pile has its own G . On doing the same kind of calculation for MCD as above, but with two different values of α , we find a matrix rank of 3, meaning that two tilts are necessary and sufficient. One group (Hierro-Rodriguez *et al.*, 2020) varied both γ and α , but they inverted the role of the two angles, using only two γ angles but scanning α . Another group (Donnelly *et al.*, 2018) performed magnetic tomography using a similar method to what's discussed here, with two tilt angles and 180 rotations. For XLD, doing the same calculation for a single polarization shows that we need three tilts. The singularity is removed with three tilts only if the polarization is neither horizontal nor vertical.

5. Conclusions and discussion

I have laid out a framework for reconstructing laminographic images of anisotropic samples under conditions of variable polarizations, as a generalization of filtered back-projection. Using this, it was possible to determine that for XLD, tomograms at at least three polarizations are required for full information to be retrieved. Alternatively, three tomograms at different tilt angles α measured at a common polarization other than horizontal or vertical provide enough information. This result is relevant for the use of dichroic tomography on beamlines whose sources are bending magnets or horizontally-polarized undulators, both of which have polarization fixed in the horizontal plane relative to gravity. Thus, to perform multi-tilt XLD tomography, the α axis must be tilted at an angle to the horizontal, i.e. β must be non-zero. For MCD, it is necessary to image at at least two tilt angles. These conditions hold even if algorithms other than filtered back-projection are used, because the back-projections hold all the information available.

In laminography, there is a loss of information in a cone in Fourier space which is, again, independent of the reconstruction method used. It is possible that constraints such as shrink-wrapping, uniaxiality (XLD) or non-negativity could help with this problem. Another possible approach is to use machine-learning techniques to constrain reconstructions to what's plausible, based

on a training set of simulated tomograms constructed to have features similar to those found in real sample. This method was used to improve signal-to-noise and reduce required dosage in tomography by (Pelt *et al.*, 2018). One may speculate that similar methods could be used to aid reconstruction in the case where an insufficient set of polarizations or tilts had been used for full recovery of the orientation. The training set must be carefully chosen so as not to impose constraints that the real sample doesn't obey.

For XLD, all of these results are contingent on the assumption that the absorption through a line in the sample may be considered to be the line integral of the local absorption along the line. The local absorption must be independent of the absorption anywhere else, a condition which requires that the polarization must be preserved as the beam propagates through the sample, something that does not happen if dichroism is strong. This problem does not occur in MCD because polarization is preserved.

Acknowledgements The author acknowledges useful discussion and encouragement from D. A. Shapiro and D. Parkinson.

References

- Chang, H., Marcus, M. A. & Marchesini, S. (2020). *Journal of Applied Crystallography* **53**, DeVol, R. T., Metzler, R. A., Kabalah-Amitai, L., Pokroy, B., Politi, Y., Gal, A., Addadi, L., Weiner, S., Fernandez-Martinez, A., Demichelis, R., Gale, J. D., Ihli, J., Meldrum, F. C., Blonsky, A. Z., Killian, C. E., Salling, C. B., Young, A. T., Marcus, M. A., Scholl, A., Doran, A., Jenkins, C., Bechtel, H. A. & Gilbert, P. U. P. A. (2014). *J. Phys. Chem. B* **118**, 8449-8457.
- Donnelly, C., Gliga, S., Scagnoli, V., Holler, M., Raabe, J., Heyderman, L. J. & Guizar-Sicairos, M. (2018). *New Journal of Physics* **20**, 083009.
- Donnelly, C., Guizar-Sicairos, M., Scagnoli, V., Gliga, S., Holler, M., Raabe, J. & Heyderman, L. J. (2017). *Nature* **547**, 328-331.
- Fischer, P. (2014). *IEEE Transactions on Magnetics* **51**, 1-31.
- Fisher, S., Holmes, D., Jørgensen, J., Gajjar, P., Behnsen, J., Lionheart, W. & Withers, P. (2019). *Measurement Science and Technology* **30**, 035401.
- Gao, Z., Holler, M., Odstrcil, M., Menzel, A., Guizar-Sicairos, M. & Ihli, J. (2020). *Chemical Communications* **56**, 13373-13376.
- Hierro-Rodriguez, A., Quirós, C., Sorrentino, A., Álvarez-Prado, L. M., Martín, J., Alameda, J. M., McVitie, S., Pereiro, E., Velez, M. & Ferrer, S. (2020). *Nature communications* **11**, 1-8.
- Lo, Y. H., Zhou, J., Rana, A., Morrill, D., Gentry, C., Enders, B., Yu, Y.-S., Sun, C.-Y., Shapiro, D. A. & Falcone, R. W. (2021). *Proceedings of the National Academy of Sciences* **118**.
- Matsuo, H., Iwata, A., Horiba, I. & Suzumura, N. (1993). *IEEE transactions on medical imaging* **12**, 307-313.
- Myagotin, A., Voropaev, A., Helfen, L., Hänschke, D. & Baumbach, T. (2013). *IEEE Transactions on Image Processing* **22**, 5348-5361.
- Pelt, D. M., Batenburg, K. J. & Sethian, J. A. (2018). *Journal of Imaging* **4**, 128.
- Rana, K. G., Seeger, R. L., Ruiz-Gómez, S., Juge, R., Zhang, Q., Pham, V. T., Belmeguenai, M., Auffret, S., Foerster, M. & Aballe, L. (2020). *arXiv preprint arXiv:2009.14796*
- Stiffler, C. A., Jakes, J. E., North, J. D., Green, D. R., Weaver, J. C. & Gilbert, P. U. (2021). *Acta Biomaterialia* **120**, 124-134.
- Stöhr, J. & Siegmann, H. C. (2006). *Solid-State Sciences. Springer, Berlin, Heidelberg* **5**,

- Van Aarle, W., Palenstijn, W. J., Cant, J., Janssens, E., Bleichrodt, F., Dabravolski, A., De Beenhouwer, J., Batenburg, K. J. & Sijbers, J. (2016). *Optics express* **24**, 25129-25147.
- van der Sluis, A. & van der Vorst, H. A. (1987). *Seismic tomography: With applications in global seismology and exploration geophysics*, edited by G. Nolet, pp. 49-83. Dordrecht: Springer Netherlands.
- Wolfram Research, I. (2021). *Mathematica*, <https://www.wolfram.com/mathematica>.
- Yu, Y.-S., Celestre, R., Enders, B., Nowrouzi, K., Padmore, H., Warwick, T., Jeong, J.-R. & Shapiro, D. A. (2018). *Microscopy and Microanalysis* **24**, 530-531.
- Zhao, D., Höchst, H. & Huber, D. L. (1998). *Journal of applied physics* **84**, 2858-2860.